Biomedical Signal Processing and Control 127 (2026) 111166

Contents lists available at ScienceDirect

Biomedical Signal Processing and Control

journal homepage: www.elsevier.com/locate/bspc

Desynchronization Index: A new connectivity approach for exploring epileptogenic networks

Federico Mason [a], Lorenzo Ferri [b,*], Lidia Di Vito [b], Lara Alvisi [c], Luca Zanuttini [c], Matteo Martinoni [b], Roberto Mai [d], Francesco Cardinale [d,e], Paolo Tinuper [c], Roberto Michelucci [b], Elena Pasini [b,1], Francesca Bisulli [b,c,1]

[a] Department of Information Engineering, University of Padova, Padova, Italy
[b] IRCCS Institute of Neurological Sciences of Bologna, European Reference Network for Rare and Complex Epilepsies (EpiCARE), Bologna, Italy
[c] Department of Neuromotor and Biomedical Sciences, University of Bologna, Bologna, Italy
[d] Claudio Munari Epilepsy and Parkinson Surgery Centre, Niguarda Hospital, Milan, Italy
[e] Department of Medicine and Surgery, University of Parma, Parma, Italy

ARTICLE INFO

Keywords:
Stereoelectroencephalography
Epilepsy
Brain connectivity
Time-varying networks
Phase transfer entropy

ABSTRACT

In drug-resistant epilepsy, Stereo-Electroencephalography (SEEG) monitoring is one of the most effective techniques to identify the Epileptogenic Zone (EZ), the fundamental prerequisite for epilepsy surgery. Despite recent technological advances, SEEG recordings remain difficult to interpret, and SEEG-guided surgery still achieves success rates below 70%. In this work, we develop a novel computational framework for SEEG analysis, with the ultimate aim of improving the accuracy in EZ definition. Specifically, we investigate the hypothesis that epileptogenic regions exhibit a tendency to behave independently and thus *desynchronize* from neighboring brain structures before seizure onset. To this end, we design the Desynchronization Index (DI), an algorithm that identifies the Epileptogenic Zone (EZ) as the subset of channels that disconnect from the SEEG network during the ictal transition. We evaluate the DI algorithm against Epileptogenicity Index (EI), one of the most common tools for EZ definition, on a clinical dataset of 20 patients, considering the channels that were thermocoagulated at the end of SEEG monitoring as the detection target. Our results show that DI overcomes EI in terms of area under the ROC curve (AUC = 0.86 vs. AUC = 0.83), while combining the two algorithms into a single framework leads to the best performance (AUC = 0.88). Overall, the DI algorithm underscores anomalous connectivity patterns that are difficult to detect through visual inspection, improving the accuracy in the EZ definition and providing new insights into the dynamics of seizure generation.

1. Introduction

The localization of the Epileptogenic Zone (EZ) is the fundamental prerequisite for performing epilepsy surgery in people with drug-resistant epilepsy [1]. Maximizing accuracy in the definition of the EZ makes it possible to reduce the extent of the surgery, mitigating the risk of complications or chronic deficits. In complex scenarios, the EZ can only be identified through invasive procedures, among which Stereoelectroencephalography (SEEG) represents the most effective solution [2]. This procedure involves the surgical implantation of electrodes into the patient's brain, enabling the recording of electrical activity from both superficial and deep cortical regions. As a result, SEEG-guided surgical resections lead more than 60% of patients to be seizure-free after the intervention [3]. However, SEEG provides very focused information: if no intracranial electrodes explore the EZ, the procedure may result in unsuccessful epilepsy surgery [4].

Nowadays, SEEG interpretation is based mainly on visual analysis, focusing on the early phases of epileptic discharge. The goal is to define an EZ that can be focal or distributed among multiple cortical structures, a scenario that falls under the concept of epileptogenic networks [5]. This process is particularly complex, since the SEEG signals include hundreds of components, named *channels*, which must be manually reviewed by highly specialized neurophysiologists. In recent years, SEEG interpretation has being supported by computational tools that aim to characterize the EZ before and during seizure generation [6]. The most common methods extract features from the SEEG power spectrum, searching for the cortical sites generating *fast*

* Corresponding author.
E-mail address: lorenzo.ferri@ausl.bologna.it (L. Ferri).
[1] Equally contributed.

https://doi.org/10.1016/j.bspc.2026.111166
Received 11 December 2025; Received in revised form 19 May 2026; Accepted 25 July 2026
Available online 3 August 2026
1746-8094/© 2026 The Authors. Published by Elsevier Ltd. This is an open access article under the CC BY license (http://creativecommons.org/licenses/by/4.0/).

oscillations [7], i.e., electrical activities with frequencies in the gamma range ($[30, 70]$ Hz), as done in the cases of EI [8] and Epileptogenic Maps (EMs) [9].

Complementary methodologies characterize SEEG signals according to the connectivity between the different channels. In this context, the first studies analyzed the responses generated through intracranial stimulations, known as Cortico-Cortical Evoked Potentials (CCEPs) [10], which, however, do not have a physiological origin. Other solutions analyze the phase distribution of the signals associated with each cortical site, as performed by the Phase Locking Value (PLV) and the Phase Lag Index (PLI), evaluating the synchrony between the SEEG channels. To estimate the direction of neural connections, we need more advanced methodologies, such as the Phase Transfer Entropy (PTE) which, notably, was applied to SEEG data only in a limited number of cases [11].

Although several connectivity approaches have been developed for the study of epileptogenic networks, the literature often presents inconsistent results. Pioneering investigations show that the *ictal phase* (i.e., the period involving epileptic discharges) is preceded by a reduction in cortical connectivity, followed by the opposite phenomenon during seizure propagation [12]. In recent years, it has been hypothesized that the EZ presents an abnormal inward information flow during the inter-ictal phase [13], and that the epileptogenic level of the cortical sites can be assessed by the strength of connections exerted after the seizure onset [14]. Notably, most recent studies follow the latter approach and characterize SEEG signals during the diffusion of epileptic discharges.

The aim of this work is to investigate whether the ability of a brain signal to evolve independently of physiological activity can serve as a key marker of epileptogenicity. From a SEEG perspective, this implies that epileptogenic channels become functionally disconnected from the rest of the SEEG network during the ictal transition. This idea is supported by prior findings [15], but, to our knowledge, has not yet been applied to quantify the epileptogenicity of individual SEEG channels. To validate our central hypothesis, we design a novel framework to support neurophysiologists in SEEG interpretation and to improve the definition of the EZ. The core of the framework is a new connectivity-based algorithm, termed DI, which identifies the EZ as the subset of SEEG channels responsible for connectivity disruptions at the seizure onset.

Overall, our main contributions consist of the following points:

- we design a new connectivity-based metric, termed *desynchronization*, describing the tendency for a SEEG channel to self-isolate from the rest of the SEEG-explored brain network;
- we design a new algorithm, named DI, which estimates the degree of epileptogenicity of cortical sites according to the increase in desynchronization during the ictal transition;
- we implement the DI algorithm to analyze seizure data in 20 patients with drug-resistant epilepsy who underwent SEEG monitoring at the IRCCS Institute of Neurological Sciences of Bologna (Italy);
- we analyze the performance of our method both against and in combination of the EI algorithm, assessing its ability to identify the SEEG channels labeled as part of the EZ during clinical evaluation.

The manuscript is organized as follows: Section 2 reports the most relevant computational tools used for SEEG interpretation; Section 3 presents the mathematical model used to represent SEEG signals and the EI algorithm; Section 4 describes the proposed DI algorithm and our evaluation methodology; Section 5 presents the results of the work; Section 6 discusses our findings from a clinical point of view; Section 7 gives the conclusions and depicts some avenues for future work.

2. Related work

In clinical practice, the interpretation of SEEG recordings constitutes a highly time-consuming process due to the huge number of data that must be visually reviewed by neurophysiologists [16]. The most common marker of the seizure onset is given by low voltage fast oscillations, which are electrical discharges spanning beta frequencies ($[13, 30]$ Hz), usually observed in mesial temporal seizures, and gamma frequencies ($[30, 100]$ Hz), observed in neocortical seizures. To quantify the magnitude of fast oscillations and, more generally, the dynamics that lead to seizures, it is common to analyze the spectrum of SEEG signals. This approach is followed by the EI algorithm [8], which is the most routinely method to assist clinicians in SEEG interpretation [17].

The EI algorithm, occasionally combined with other biomarkers [18], has been recognized to provide the best accuracy in terms of EZ localization and surgical prediction. An extension of such an approach is the *epileptogenicity rank*, a technique that, before computing the EI values, assigns weights to the SEEG sites depending on their distance from the hypothesized target of the EZ [19]. However, this solution biases the epileptogenic levels assigned to each channel by a prior assumption. In particular, the epileptogenicity rank reduces the number of false positives when the clinical hypothesis is correct, but dramatically decreases the sensitivity in the other case.

While EI focus on the energy distribution in the frequency domain, other approaches analyze the variation in signal synchronization. Several tools have been proposed for this purpose, including the PLV [20] and the PLI [21], with different trade-offs in terms of sensitivity and precision [22]. Notably, the PLI was proposed as an alternative to the PLV in order to mitigate the noisy information associated with *volume conduction* [23]. A more advanced method is the PTE [24], which allows us to estimate both the delay and the direction of neural connections, representing a promising yet underutilized technique for SEEG analysis [11].

In one of the first works in this field, Bartolomei et al. exploit the nonlinear regression coefficient (h2) [25] and show that the EZ is associated with reduced connectivity at the beginning of the ictal phase [15]. On the other hand, recent literature primarily characterizes the EZ after the seizure onset, with the epileptogenic levels of SEEG channels quantified in terms of functional connectivity during the ictal phase [26,27]. Two examples are provided in [28], where functional connectivity is integrated with the Euclidean distance, and [29], where graph theory is used to identify network hubs during seizure propagation.

More advanced connectivity-based approaches associate the phase of slow oscillations with the amplitude of fast oscillations, as occurred for the Phase Slope Index (PSI) and the Phase Amplitude Coupling (PAC) methods [30]. In this regard, the authors of [31] exploit PSI to analyze SEEG signals and confirm that epileptogenic channels show increased outward connectivity during the ictal phase. Similar observations are presented in [32], whose authors computed the PAC between the high (gamma) and low (delta and theta) frequency bands. However, a recent work [33], using Partial Direct Coherence (PDC) [34] as a connectivity measure, contradicts these findings and reports that the EZ presents greater inward connectivity during seizure propagation.

Despite the large variety of works that use connectivity-based metrics for the interpretation of SEEG signals, the results in the literature do not lead to an agreement on how to characterize the EZ. Initial studies suggest that the ictal transition is characterized by a reduction in connectivity, which is consistent with the desynchronization hypothesis proposed in this work. In contrast, more recent approaches identify the EZ as the subset of cortical sites exhibiting stronger coupling during seizure propagation. These discrepancies may depend on the specific filtering pipeline used to analyze SEEG data, as epileptogenic signals may lead to higher functional connectivity in high-frequency bands while reducing it within physiological frequency ranges.

3. Mathematical preliminaries

In this section, we first describe how single SEEG channels are modeled within our framework and define the *energy ratio* as a baseline epileptogenicity biomarker. Then, we formulate the connectivity model used to infer the relation between SEEG sites starting from their phase distribution. Finally, we introduce the EI algorithm, which represents the state-of-the-art for defining the EZ and will serve as a benchmark for the evaluation of our computational framework.

3.1. Channel model

We model an SEEG recording as a multidimensional signal with multiple channels, one for each cortical site analyzed. In the rest of the paper, we denote by $\mathcal{N}$ the set of channels and by $|\cdot|$ the cardinality operator, so that the number of cortical sites explored by the SEEG implant is $N = |\mathcal{N}|$. In our model, each channel $x \in \mathcal{N}$ is segmented in multiple overlapping windows $x(t)$, with $t = 0, \Delta t, 2\Delta t, \ldots$, where Δt represents the time-shift between consecutive windows. In particular, given the duration T_{window} of a single window and the sampling frequency f_s, the number of samples per window is $n = T_{\text{window}} \cdot f_s$.

Baseline approaches to quantifying the epileptogenicity of SEEG channels rely on analyzing the distribution of signal energy in the frequency domain. To obtain a frequency-domain representation of $x(t)$, we apply the Fourier Transform (FT), obtaining a complex value $X(t, f)$ for each frequency in $[0, f_s/2]$. Following the approach proposed in [8], we then compute the *energy ratio* between the high- and low-frequency bands of $x(t)$ as

$$E_x(t) = \frac{\int_{B_h} \|X(t,f)\|^2 df}{\int_{B_\ell} \|X(t,f)\|^2 df}, \tag{1}$$

where B_h and B_ℓ are the high- and low-frequency ranges, while $\|\cdot\|$ is the norm function. The straightforward idea behind the energy ratio is that epileptic discharge is characterized by an increase in fast oscillations and a concurrent decrease in slow oscillations. By normalizing the high-frequency energy by the low-frequency energy, we can fairly compare the signals recorded at different cortical sites, which may be characterized by different total energy.

3.2. Connectivity model

To estimate the relations between different SEEG channels, we consider the PTE, which models the coupling of any pair of channels $x, y \in \mathcal{N}$ according to their phase distributions. Given a specific window $x(t)$, we first calculate its *analytic representation* $x_a(t) = x(t) + jHT(x(t))$, where $HT(\cdot)$ is the Hilbert transform. We observe that $x_a(t)$ is associated with $n = T_{\text{window}} \cdot f_s$ phase values, which constitute the *instantaneous phase* $\theta_x(t) \in [-\pi, +\pi]$ of channel x at time t and provide information about the signal's cycle position independently of its amplitude. Notably, in this manuscript, we do not apply any filtering before the Hilbert transform, so $\theta_x(t)$ represents the phase of the broadband signal associated with channel x. Extending the approach to specific frequency ranges is also possible and will be investigated in future work.

To model the phase distribution, we use an histogram with uniform bin widths. Hence, we follow the Sturges rule [35] and compute the width of each bin as $\vartheta = 2\pi/(\log_2(n) + 1)$. We observe that the width of each bin increases with the domain of the target variable, which, in the case of a phase, is equal to 2π, and decreases with the number of samples, which in our model is fixed and equal to n. This quantization step reduces the sensitivity to zero-lag coupling, attenuating the biases associated with volume conduction.[2]

[2] Another approach designed to mitigate volume conduction is the PLI algorithm, which evaluates neural synchronization by considering only the sign of phase differences. However, PLI does not allow us to measure the direction of the information flows between signals [21] and underestimates neural connections with phase difference that fluctuates around zero. The opposite approach is taken by PLV, which models the phase in a continuous domain, resulting more sensitive to both genuine and spurious zero-lag coupling connections.

Let us denote by $\theta_x(t)$ and $\theta_y(t)$ the phase distribution of $x(t)$ and $y(t)$, respectively. According to the PTE, the strength of the connections that channel x exerts on channel y at time t, considering a lag τ, is given by

$$\begin{aligned} T_{x\to y}(t,\tau) = H\left(\theta_y(t), \theta_y(t+\tau)\right) + \\ H\left(\theta_x(t), \theta_y(t)\right) - H\left(\theta_x(t), \theta_y(t), \theta_y(t+\tau)\right) - H\left(\theta_y(t)\right), \end{aligned} \tag{2}$$

where $H(\cdot)$ denotes the Shannon entropy function. Intuitively, $T_{x\to y}(t,\tau)$ represents the amount of information that $\theta_y(t+\tau)$ shares with $\theta_x(t)$ and that cannot be predicted from the past of values of θ_y.

We observe that the PTE is a directed connectivity measure, which means that, in general, $T_{x\to y}(t,\tau) \neq T_{y\to x}(t,\tau)$. In order to remove the dependency from τ, with a slight abuse of notation, we redefine the PTE between $x(t)$ and $y(t)$ as the maximum value of $T_{x\to y}(t,\tau)$ among multiple lags in the set $[0, \tau_{max}]$:

$$T_{x\to y}(t) = \max_{\tau\in[0,\tau_{max}]} T_{x\to y}(t,\tau). \tag{3}$$

By doing so, we obtain that the magnitude of the effective connection exerted on channel y by channel x at time t is given by $T_{x\to y}(t)$, while the propagation delay associated with such a connection is:

$$\tau_{x\to y}(t) = \arg\max_{\tau\in[0,\tau_{max}]} T_{x\to y}(t,\tau). \tag{4}$$

We observe that if $\tau_{x\to y}(t) = 0$, there is a zero propagation delay for the information flow going from $x(t)$ to $y(t)$.

3.3. Epileptogenicity index

The EI algorithm considers the energy ratio as a biomarker for identifying abnormal channels during the ictal transition and, consequently, defining the EZ. However, EI is not designed to simply assign higher epileptogenicity values to channels with higher energy ratios, as high-frequency oscillations can occur even in the absence of epileptic discharges. To address this issue, the EI algorithm implements a CUmulative SUM (CUSUM) control chart to discern physiological from epileptogenic signals. Given a sequence of observations $\omega(t)$, interspersed by a period Δt, the CUSUM chart is defined by the function

$$\Gamma(\omega,t) = \begin{cases} \max\left\{0, \Gamma(\omega, t-\Delta t) + \frac{\omega(t)-\mu_\omega}{\sigma_\omega} - \gamma\right\}, & t > 0; \\ \omega(t), & t = 0; \end{cases} \tag{5}$$

where $\gamma \in \mathbb{R}$ is a tuning parameter that makes the statistic less or more sensitive to the new observations, while μ_ω and σ_ω are the estimates of the mean and standard deviation of ω. In the case of the EI algorithm, the observations $\omega(t)$ are given by the energy ratios $E_x(t)$ associated the SEEG channels $x \in \mathcal{N}$.

The original version of the EI algorithm does not consider the standard deviation in the normalization process, and dynamically re-estimates the mean energy ratio every time the energy ratio varies significantly. In this manuscript, we estimate the baseline statistic of each channel $x \in \mathcal{N}$ by looking at the period immediately preceding the ictal discharge. In particular, we compute μ_{E_x} and σ_{E_x} over the interval $\{t_{\text{base}}, \ldots, t_{\text{start}}\}$, where t_{start} is the instant that corresponds to the seizure onset. Then, we compute the cumulative sum $\Gamma(E_x, t)$ of the energy ratio $E_x(t)$ for each time $t \in \{t_{\text{start}}, \ldots, t_{\text{end}}\}$, where t_{end} is the instant at which epileptic discharge have propagated within the whole brain.

Given a channel $x \in \mathcal{N}$ and $\Gamma(E_x, t)$, we define the *activation time* as the instant of time at which $\Gamma(E_x, t)$ reaches the highest value:

$$t_{E_x} = \underset{t \in \{t_{\text{start}}, \ldots, t_{\text{end}}\}}{\arg\max} \; \Gamma(E_x, t) \tag{6}$$

Hence, we define the *cumulative energy* of the channel as the sum of the energy ratio E_x over the period following the channel's activation time:

$$c_{E_x} = \sum_{t=t_{E_x}}^{t_{E_x}+m\cdot\Delta t} E_x(t), \tag{7}$$

where $m \in \mathbb{Z}^+$ is the number of windows over which c_{E_x} is calculated. Notably, the latter coincides with the integral of the energy ratio over a given time period and represents the magnitude of the abnormality of channel x, quantified in terms of the increase of high-frequency oscillations.

Finally, EI identifies the EZ as the group $\mathcal{N}_E$ of channels with the strongest variations in the energy ratio, that is

$$\mathcal{N}_E = \left\{ x \in \mathcal{N} \,:\, \Gamma(E_x, t_{E_x}) > \eta \cdot \max_{y,t} \Gamma(E_y, t) \right\}, \tag{8}$$

where $\eta \in [0, 1]$ is the *detection threshold*. The epileptogenicity level of each channel $x \in \mathcal{N}$ is $EI_x = 0$, $\forall\, x \in \mathcal{N} \setminus \mathcal{N}_E$, and

$$EI_x = \frac{c_{E_x}}{t_{E_x} - t_{\text{start}}}, \; \forall x \in \mathcal{N}_E. \tag{9}$$

We observe that EI_x is proportional to c_{E_x} and decreases as a function of the difference between t_{E_x} and t_{start}, i.e., the time delay with which channel x begins to exhibit high-frequency oscillations relative to seizure onset.

We note that our formulation stands out from the original EI algorithm by reducing the number of parameters to be manually set. The times t_{start} and t_{end} denote the period during which epileptic discharges are generated, while t_{base} must ensure that μ_{E_x} and σ_{E_x} capture the baseline brain activity of the patient. The only parameters to be manually tuned are the number m of windows over which c_{E_x} is computed, the weight γ of the CUSUM control chart, and the threshold η which, notably, trades off false alarms and miss-detections.

4. Methodology

In this section, we present our novel detection algorithm, the Desynchronization Index (DI), which is designed to quantify the epileptogenic level of SEEG channels based on their tendency to self-isolate from the SEEG network during the ictal transition. We then describe the pipeline used to evaluate our approach, including the SEEG recording process, the clinical dataset, and the metrics used to assess the performance of the overall detection framework.

4.1. Desynchronization index

The DI algorithm is built on a novel epileptogenicity biomarker, termed *desynchronization*, which characterizes epileptogenic channels according to their reduced connectivity with respect to the rest of the SEEG network. To design this biomarker, we consider a similar approach to [36], where the goal is to detect anomalous nodes in time-varying networks.

Following the model in Section 3.2, we write $\mathcal{T}(t)$ to indicate the distribution of connections $T_{x\to y}(t)$, $\forall\, x, y \in \mathcal{N}$, in the SEEG network at time t, and $\mathcal{T}_n(t)$ to denote the nth percentile of the distribution. Hence, to separate genuine from spurious interactions, we define $\mathcal{N}_x^{\text{low}}(t)$ and $\mathcal{N}_x^{\text{high}}(t)$ as the sets of channels that exhibit significantly reduced and increased information flow originating from channel x:

$$\mathcal{N}_x^{\text{low}}(t) = \left\{ y \in \mathcal{N} \,:\, T_{x\to y}(t) \le \mathcal{T}_{n_{\text{low}}}(t) \right\}, \tag{10}$$

$$\mathcal{N}_x^{\text{high}}(t) = \left\{ y \in \mathcal{N} \,:\, T_{x\to y}(t) \ge \mathcal{T}_{n_{\text{high}}}(t) \right\}. \tag{11}$$

In other words, a connection is deemed significant if its strength lies below the n_{low}th or exceeds the n_{high}th percentile of the time-varying network distribution. This allows us to implicitly customize the framework to each patient without the need to define additional hyperparameters, which is a strong limitation in [36]. We observe that other rules for discerning significant connections could lead to different trade-offs in terms of accuracy, and further investigation of how to tune n_{low} and n_{high} will be part of our future work.

We now define the actual $\psi_x^{\text{low}}(t)$ and awaited $\hat{\psi}_x^{\text{low}}(t)$ densities of low-strength connections originating from channel x as

$$\psi_x^{\text{low}}(t) = \sum_{y \in \mathcal{N}_x^{\text{low}}(t)} T_{x\to y}(t), \tag{12}$$

$$\hat{\psi}_x^{\text{low}}(t) = |\mathcal{N}_x^{\text{low}}(t)| \cdot \mathcal{T}_{n_{\text{low}}}(t). \tag{13}$$

Similarly, we define the actual $\psi_x^{\text{high}}(t)$ and awaited $\hat{\psi}_x^{\text{high}}(t)$ densities of high-strength connections originating from channel x as

$$\psi_x^{\text{high}}(t) = \sum_{y \in \mathcal{N}_x^{\text{high}}(t)} T_{x\to y}(t), \tag{14}$$

$$\hat{\psi}_x^{\text{high}}(t) = |\mathcal{N}_x^{\text{high}}(t)| \cdot \mathcal{T}_{n_{\text{high}}}(t). \tag{15}$$

Hence, $\psi_x^{\text{low}}(t)$ is proportional to the cumulative magnitude of low-strength outward connections of channel x, while $\psi_x^{\text{high}}(t)$ is proportional to the cumulative magnitude of high-strength outward connections of the same channel. By definition, we always have $\psi_x^{\text{low}}(t) < \hat{\psi}_x^{\text{low}}(t)$ and $\psi_x^{\text{high}}(t) > \hat{\psi}_x^{\text{high}}(t)$.

We define the desynchronization $D_x(t)$ of channel $x \in \mathcal{N}$ at time t as

$$D_x(t) = \frac{\sqrt{\hat{\psi}_x^{\text{low}}(t)} - \sqrt{\psi_x^{\text{low}}(t)}}{\epsilon + \sqrt{\psi_x^{\text{high}}(t)} - \sqrt{\hat{\psi}_x^{\text{high}}(t)}}, \tag{16}$$

where the square root operator is used to stabilize the variance of the process [36], and $\epsilon > 0$ is a small constant to avoid numerical stability in edge cases. The denominator of the above equation decreases as x presents a lower number of high-strength outward connections, while the numerator increases as x presents a higher number of low-strength outward connections. Therefore, $D_x(t)$ represents the tendency of x to self-isolate from the rest of the network.

We observe that both the denominator and the numerator of Eq. (16) always take positive values and, consequently, $D_x(t) \in \mathbb{R}^+$, $\forall\, x \in \mathcal{N}$. In the edge case, a node x may present only null-value connections, which leads $\hat{\psi}_x^{\text{high}}(t) = \psi_x^{\text{high}}(t) = \psi_x^{\text{low}}(t) = 0$, $\hat{\psi}_x^{\text{low}}(t) = N \cdot \mathcal{T}_{n_{\text{high}}}(t) > 0$, and, consequently, $D_x(t) \to +\infty$. This numerical instability is avoided by the constant $\epsilon > 0$ in the denominator, ensuring that $D_x(t)$ is upper bounded by $(N \cdot \mathcal{T}_{n_{\text{high}}}(t))^{1/2} \cdot \epsilon^{-1} \le (N \cdot T_{\max})^{1/2} \cdot \epsilon^{-1}$, where $T_{\max}$ is the maximum PTE value.

To identify epileptogenic channels, DI follows the same approach as EI, monitoring which channels exhibit the most prominent desynchronization changes during the ictal transition. Using the pipeline presented in Section 3.3, we apply the CUSUM chart and obtain $\Gamma(D_x, t)$ for each channel $x \in \mathcal{N}$ and for each time t between t_{start} and t_{end}. Hence, using Eqs. (6) and (7), we compute the activation times t_{D_x} and the cumulative desynchronization c_{D_x}, $\forall\, x \in \mathcal{N}$. Finally, we define $\mathcal{N}_D$ as the set of channels that show the strongest changes in terms of desynchronization, and compute the DI value of each channel $x \in \mathcal{N}_D$ as the ratio between c_{D_x} and the delay of channel's activation:

$$\mathcal{N}_D = \left\{ x \in \mathcal{N} \,:\, \Gamma(D_x, t_{D_x}) > \eta \cdot \max_{y,t} \Gamma(D_y, t) \right\}, \tag{17}$$

$$DI_x = \begin{cases} \dfrac{c_{D_x}}{t_{D_x} - t_{\text{start}}} & x \in \mathcal{N}_D, \\ 0 & x \notin \mathcal{N}_D. \end{cases} \tag{18}$$

The DI algorithm presents the same hyperparameters of EI, making it necessary to tune only the threshold $\eta \in [0, 1]$, the number m of

Table 1
Demographic and clinical data.

Patient index	Sex	Age (SEEG)	Age (onset)	Seizure frequency	Epileptogenic zone localization	Surgery	Outcome (1 year)	Histology
1	Male	36	9	Weekly	Right temporo-occipital	Cortectomy	Engel II	N/A
2	Female	49	12	Monthly	Left temporal	Lobectomy	Engel I	HS 1
3	Male	48	7	Annual	Right frontal	RF-TC	Engel II	N/A
4	Female	25	2	Weekly	Right temporo-basal	Lobectomy	Engel I	Gliosis
5	Female	26	12	Weekly	Left temporal	RF-TC	Engel I	N/A
6	Male	39	33	Weekly	Right temporal	Lobectomy	Engel I	HS 1
7	Female	31	13	Daily	Right orbito-frontal	RF-TC	Engel I	N/A
8	Male	24	1	Daily	Left orbito-frontal	RF-TC	Engel I	FCD
9	Male	32	16	Monthly	Right temporal	RF-TC	Engel II	N/A
10	Male	30	12	weekly	Left temporo-basal	RF-TC	Engel II	N/A
11	Female	34	22	Monthly	Left temporo-occipital	RF-TC	Engel I	N/A
12	Female	29	2	Daily	Right insular	RF-TC	Engel II	N/A
13	Female	43	37	Monthly	Right temporal	RF-TC	Engel I	N/A
14	Male	36	16	Monthly	Left temporal	Lobectomy	Engel I	FCD
15	Female	50	3	Monthly	Right temporal	Lobectomy	Engel I	HS 1
16	Male	19	5	Monthly	Right temporal	RF-TC	Engel I	N/A
17	Male	32	16	Daily	Left insular	RF-TC	Engel I	N/A
18	Female	38	13	Monthly	Right temporo-occipital	RF-TC	Engel I	N/A
19	Male	24	18	Weekly	Right temporal	RF-TC	Engel I	Tumor
20	Male	48	22	Weekly	Right temporal	Lobectomy	Engel I	HS 1

windows to compute the cumulative desynchronization, and the weight γ of the CUSUM chart.

We observe that the threshold η establishes the channels included in the EZ, i.e., the composition of $\mathcal{N}_D$, while DI_x is used to assess the importance of the different channels within the EZ itself. In the original work by Bartolomei and colleagues [8], an additional threshold was applied to the index values to distinguish propagator channels from truly epileptogenic ones. In this work, we avoid introducing this additional detection level in order to enhance the explainability of the framework and to focus exclusively on determining which feature, energy ratio or desynchronization, is more suitable for defining the EZ.

4.2. Clinical dataset

This work considers an initial cohort of 24 consecutive patients that have been monitored through SEEG at the IRCCS Institute of Neurological Sciences of Bologna from January 2022 to September 2025. The study protocol was approved by the local ethics committee (protocol number 25058, committee code 97338), and written informed consent was obtained from each patient.

Before implantation, all patients underwent a comprehensive non invasive presurgical evaluation, including long-term video-EEG, 3T brain magnetic resonance imaging, neuro-psychological assessment, and FDG-PET. The findings of these non-invasive examinations were then integrated to formulate the localization hypothesis for the EZ, which subsequently guided SEEG electrode planning. The SEEG implantation followed the workflow developed at Niguarda Hospital [37], which involves the construction of a multimodal scene of the patient's brain. The scene allowed for a comprehensive evaluation of all the anatomical information regarding the cortical area explored by each contact.

Each SEEG implant included multiple electrodes and each electrode had 5–18 recording sites, corresponding to the channels of the recorded signal. The number and location of the electrodes were tailored per patient, while each contact was 22 mm in length, and separated by 1.5 m from neighboring contacts. The SEEG signals were recorded using the Nihon Kohden 2100 polygraph, considering 192 or 256 channels and a sampling frequency of $f_s = 1000$ Hz. High-definition synchronized videos were recorded throughout each SEEG monitoring (up to 20 days), enabling the correlation between electrical and clinical features.

From the initial cohort, we excluded 4 patients who did not achieve seizure control. The final population comprised 11 males and 9 females with an average age of 34 years (range 19–50) at the time of recording, and 12 years (range 1–37) at the onset of the disease. Clinical evaluation of the SEEG signals localized the EZ in the temporal lobe in 10 cases (7 right, 3 left), temporo-occipital region in 3 cases (2 right, 1 left), temporo-basal region in 2 cases (1 right, 1 left), insular lobe in 2 cases (1 right, 1 left), orbito-frontal region in 2 cases (1 right, 1 left), and right frontal lobe in 1 case.

After one year of follow-up, seizure control was achieved in 13 patients (9 Engel I, 4 Engel II) who underwent Radio Frequency Thermocoagulation (RFTC), 6 patients (Engel I) who underwent temporal lobectomy, and a single patient who underwent cortectomy (Engel II). Histopathological analysis revealed findings compatible with Hippocampal Sclerosis (HS) in 4 cases and Focal Cortical Dysplasia (FCD) in 2 cases. The demographic and clinical details of the overall population are reported in Table 1.

4.3. Analysis pipeline

To build the signal dataset, we select a single seizure per patient and analyze an SEEG epoch of $T_{\text{epoch}} = 200.0$ seconds for each seizure. When multiple ictal events are available, we discard seizures recorded during the first two days of the monitoring period and those occurring within a seizure cluster, and select the first seizure among the remaining ones. For each epoch, we set the start time so that the seizure onset occurs at $t_{\text{start}} = 170.0$ seconds, allowing us to consistently study the ictal transition across the entire population.

Before running the EI and DI algorithms, we process the SEEG signals through a comb filter centered at $f_{\text{comb}} = 50$ Hz to suppress the powerline frequency and its harmonics. In this phase, we remove SEEG channels that exhibit recording artifacts, including voltage saturation and other forms of signal distortion. Notably, the labeling of *bad channels* was performed by the clinicians during routine visual inspection of SEEG recordings. No other cortical sites are excluded, ensuring that the proposed computational framework remains independent of both patient-specific and seizure-specific factors.

We recall that the outputs of the EI and DI algorithms consist of the subset of SEEG channels classified as epileptogenic. To establish a clinical ground truth, we selected channels that underwent RFTC, as in our population this procedure was applied to all channels clinically identified as part of the EZ. Hence, for each epoch in the dataset, we implement the EI and DI algorithms both as standalone tools and in a joint configuration. In the latter case (named "EI and DI"), a channel is classified as epileptogenic when at least one of the algorithms identifies it as positive. For a fixed detection threshold η, the "EI and DI" system

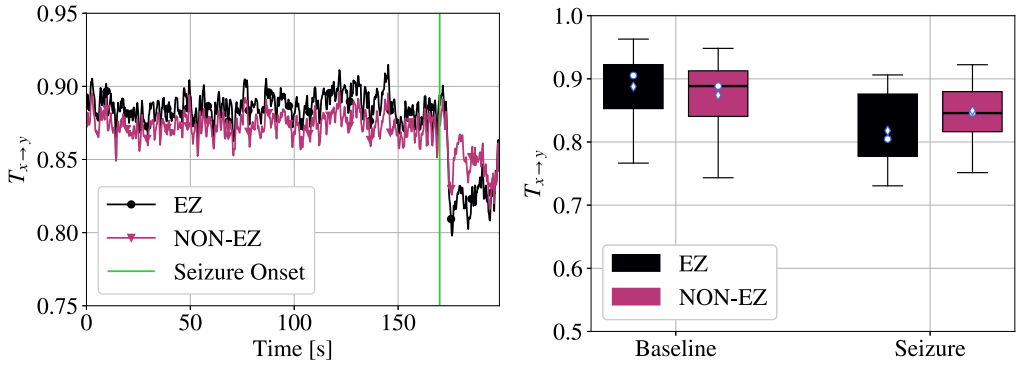

(a) Connectivity in time.

(b) Connectivity distribution.

Fig. 1. Outward connectivity during the ictal transition.

is expected to improve sensitivity, at the cost of an increased number of false positives.

To assess the performance of the algorithms and their combination, we compute, for each epoch in the dataset, the following metrics:

- *Sensitivity* (or *true positive rate*), which is the ratio between the number of channels correctly classified as epileptogenic by the algorithm and the total number of epileptogenic channels in the SEEG implant;
- *Precision* (or *positive predictive value*), which is the ratio between the number of channels correctly classified as epileptogenic and the total number of channels classified as epileptogenic by the algorithm;
- *F1 score*, which is defined as the harmonic mean of precision and recall and provides a balanced measure of a model's ability to correctly identify epileptogenic channels while accounting for false positives.

Furthermore, to study the trade-off between sensitivity and precision, we calculate the Receiver Operating Characteristic (ROC) and the Area Under the ROC Curve (ROC-AUC). The ROC-AUC is a common performance indicator for diagnostic tools: in clinical settings, a value greater than 0.80 is required to obtain a reliable solution [38]. To ensure that the detection performance is not biased by the low number of positive elements, we also computed the Area Under the Precision-Recall Curve (PR-AUC). This metric is particularly informative for imbalanced dataset, where the ROC-AUC can appear artificially high.

The computational framework used to process the SEEG data and obtain the results of this manuscript is publicly available at the link: https://github.com/masonfed/desync_index.

5. Results

In this section, we evaluate the performance of the EI and DI algorithms to define the EZ, considering the analysis pipeline given in Section 4.3. In particular, we first conduct an exploratory analysis to assess how SEEG connectivity changes within the EZ during the ictal transition. We then analyze in detail two representative seizure events, highlighting the differences between EI and DI for detecting epileptogenic channels. Finally, we examine the detection results aggregated across the entire patient population.

5.1. Exploratory analysis

Each SEEG epoch is segmented in overlapping time windows lasting $T_{\text{window}} = 1.0$ s each, considering a time shift of $\Delta t = 0.25$ s between consecutive windows. Thus, given the epoch duration ($T_{\text{epoch}} = 200.0$ s) a total of 797 windows is analyzed for each seizure. For computing the energy ratio, the high and low frequency ranges are set to $B_h = [30.0, 250.0]$ Hz and $B_\ell = [4.0, 14.0]$ Hz, respectively. We thus extend the portion of the spectrum processed by the EI algorithm, whose initial version considered frequencies lower than 97 Hz [8]. By considering a wider frequency range, we can capture *ripple* phenomena that are notably characterized by oscillations up to 250 Hz or even more [39].

For computing the desynchronization values, we consider $\tau_{max} = 0.25$ s as the maximum propagation delay, and $n_{\text{low}} = 5$ and $n_{\text{high}} = 95$ to discern significant and spurious interactions in the SEEG network. Hence, we compute c_{E_x} and c_{D_x} over $m = 20$ windows, as done in [8], and we set the weight of the CUSUM chart to $\gamma = 0$, following the recommendations provided in [40]. We set the start time of the baseline period to $t_{\text{base}} = t_{\text{start}} - 100.0$ s, and the end time of the detection procedure to $t_{\text{end}} = t_{\text{start}} + 20.0$ s. As explained in Section 4, t_{start} coincides with the seizure onset and is equal to 170.0 s.

Before considering detection performance, we characterize the EZ and the rest of the SEEG network in terms of outward connectivity. Fig. 1(a) represents the mean outward connectivity for EZ and NON-EZ channels, over the 200.0 s analyzed with the results averaged across the entire population. The EZ is associated with a greater outward connection than the rest of the network before the seizure onset ($t < t_{\text{start}}$). Instead, after the start of epileptic discharges, both epileptogenic and non-epileptogenic channels present a drop in connectivity, which, in the case of the EZ, goes from ≈ 0.9 to ≈ 0.8.

In Fig. 1(b), we represent the distribution of the mean outward connectivity $T_{x\to y}$ of each channel x within the EZ and NON-EZ before and after t_{start}. In particular, we consider the interval $\{t_{\text{base}}, \dots, t_{\text{start}}\}$ as the baseline and the interval $\{t_{\text{start}} + 5.0\text{ s}, \dots, t_{\text{start}} + 15.0\text{ s}\}$ as the seizure period. By performing a one-sided two-sample t-test ($\alpha = 0.05$), we prove that this connectivity outage is strongly significant for the EZ (p-value < 0.001) and marginally significant for the rest of the SEEG network (p-value $= 0.063$). These results suggest that outward connectivity is particularly effective in identifying epileptogenic channels and support the use of the DI algorithm as a tool for precise EZ localization.

5.2. Concordant example

In the following, we focus on the operative characteristics of the EI and DI algorithms, illustrating how each identifies EZ channels in two representative seizure events. We first consider patient 1, whose SEEG implant (represented in Fig. 2(a)) explores the right temporo-parietal and occipital areas, including 189 different recording sites (18 electrodes). Fig. 3(a) reports the bipolar representation of the channels that are identified as epileptogenic by the EI algorithm when setting $\eta = 16\%$, while Fig. 3(b) represents the energy ratios associated with each of those channels. In the two figures, t_{start} denotes the seizure

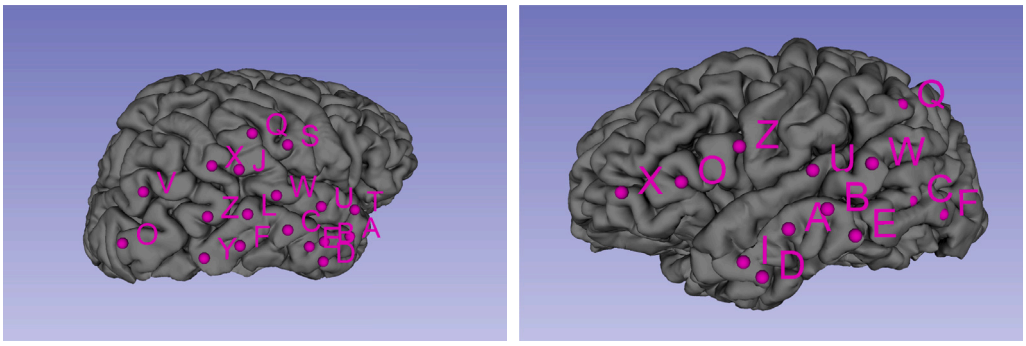

(a) Patient 1. (b) Patient 2.

Fig. 2. SEEG implants.

onset, while the markers t_x denote the times at which the energy ratio E_x diverges from its baseline.

In Fig. 4, we investigate the results of the DI algorithm in the same scenario. To ensure a fair comparison of the operative behavior of the algorithms, we set $\eta = 40\%$, so that DI identifies the same number of epileptogenic channels as reported by EI. This allows us to examine how the algorithms select channels, regardless of differences in output size. Finally, Fig. 5 reports the epileptogenicity levels assigned to each channel by the two algorithms, as well as the brain structure with which each channel is associated. In both cases, the indices are normalized within the $[0, 1]$ range, such that values close to 1 indicate a greater influence on the generation of epileptic discharge.

Overall, the results are largely concordant: both algorithms locate the seizure triggers within the lingual gyrus, the collateral sulcus and the fusiform gyrus. Notably, all these regions were clinically identified as part of the EZ and were thermocoagulated at the end of SEEG monitoring. In particular, the target patient underwent a cortectomy of the right lingual and fusiform gyri,[3] which results in a favorable seizure outcome (Engel II).

In detail, Figs. 3(b) and 5(a) show that EI seems to identify channel $Y3$ as the primary epileptogenic focus. Hence, $Y3$ visually exhibits the most abnormal energy variation after seizure onset ($t > 170.0$ s), and its EI value exceeds that of all other channels by more than 50%. Figs. 4(b) and 5(b) indicate that DI produces more diffuse outputs, with significant abnormal connectivity patterns distributed across channels $Y7$–$Y11$ and $F2$–$F4$, all of which report significant DI values. However, the channel that exhibits the most prominent variation is still $Y3$, confirming its central role in originating epileptic discharges.

5.3. Discordant example

In the following, we consider patient 2, whose SEEG implant (shown in Fig. 2(b)) explores the left temporo-parietal and frontal areas and includes 163 recording sites (13 electrodes). Figs. 6 and 7 report the channels considered the most epileptogenic according to the two algorithms together with the associated energy ratio and desynchronization values. As before, the detection threshold η was tuned to obtain the same number of outputs in the two cases, thus enabling a fair performance comparison. Finally, Fig. 8 compares the epileptogenicity levels assigned by the two algorithms and the channel locations within the SEEG implant.

Figs. 6(b) and 8(a) indicate that EI identifies channels $I1$–$I2$, exploring the mesial temporal pole, as the origin of epileptic discharges, being the only channels with prominent epileptogenicity values. In contrast, Figs. 7(b) and 8(b) show that DI produces more diffuse outputs, assigning elevated epileptogenicity values to multiple channels within the limbic system. In particular, DI identifies epileptogenic phenomena in channels $C2$ and $B3$, which both explore the hippocampus and, critically, were not labeled as part of the EZ by the EI algorithm.

As indicated by Table 1, the target patient (patient 2) was diagnosed with hippocampal sclerosis and achieved seizure freedom only after the removal of both amygdala (channels $A1$-$A3$) and the hippocampus (channels $B1$-$B3$ and $C1$-$C3$). This outcome suggests that, in this specific scenario, relying solely on the energy ratio could increase the risk of false negative errors. Therefore, integrating both energy- and connectivity-based biomarkers is essential to improve accuracy in the EZ definition and, consequently, the likelihood of seizure freedom.

5.4. Aggregate results

In the following, we analyze the performance of the EI and DI algorithms across the entire patient population. In particular, we consider each algorithm as a standalone tool, as well as their combination (EI and DI), in which a channel is considered part of the EZ if it is identified as positive by either EI or DI. Fig. 9 reports the detection performance of the algorithms while setting $\eta = 5\%$ and $\eta = 10\%$ as detection threshold. In the first case, DI increases the sensitivity by 11.5% compared to EI (0.68 vs 0.61), while the algorithm combination achieves a score of 0.72. This indicates that two algorithms produce different results and the channels with higher EI values do not necessarily correspond to those with higher DI values. Focusing on the F1 score, the DI algorithm outperforms both the benchmark and the joint configuration, achieving F1 score = 0.46.

To improve precision, we can increase the threshold η, thus reducing the number of channels classified as part of the EZ. Fig. 9(b) reports the results for $\eta = 10\%$, showing that the EI and the DI algorithms yield precisions of 0.50 and 0.53, respectively. Taking into account the F1 score, DI improves performance compared to the previous scenario (F1 score = 0.49) and still represents the best solution. On the other hand, EI and DI lead to F1 score = 0.39 and F1 score = 0.46, respectively. We observe that the relatively low F1 scores are mainly due to the need to adjust the detection threshold η individually for each patient, based on the extent of their SEEG implantation.

To analyze the trade-off between sensitivity and specificity, we consider the average ROC-AUC across the clinical dataset. Fig. 10(a) denotes how the algorithm combination leads to the highest detection performance, with a final score of ROC-AUC = 0.88, while the standalone algorithms yield ROC-AUC = 0.86 for DI and ROC-AUC = 0.83 for EI. In particular, combining EI and DI improves the ROC-AUC score by 5.2% with respect to the EI algorithm (95% confidence interval: 2.3%–8.0%), enabling a more precise characterization of the ictal transition. The benefit of integrating the two approaches is confirmed from the comparison of precision and the recall scores, as shown in Fig. 10(b). The combined algorithm achieves PR-AUC = 0.53, which is

[3] We specify that these clinical details are not derived from Tab. I, which only reports the coarse EZ localization, but are based on the surgical reports associated with the patient.

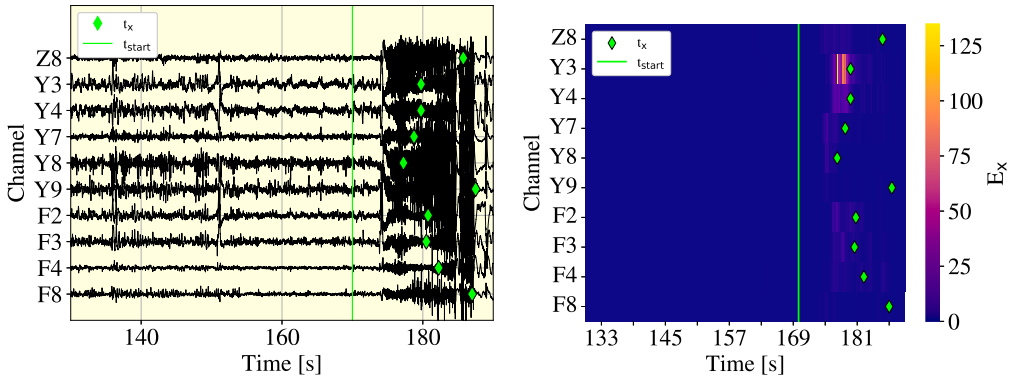

(a) Signal. (b) Energy ratio.

Fig. 3. The EI algorithm (patient 1, $\eta = 16\%$).

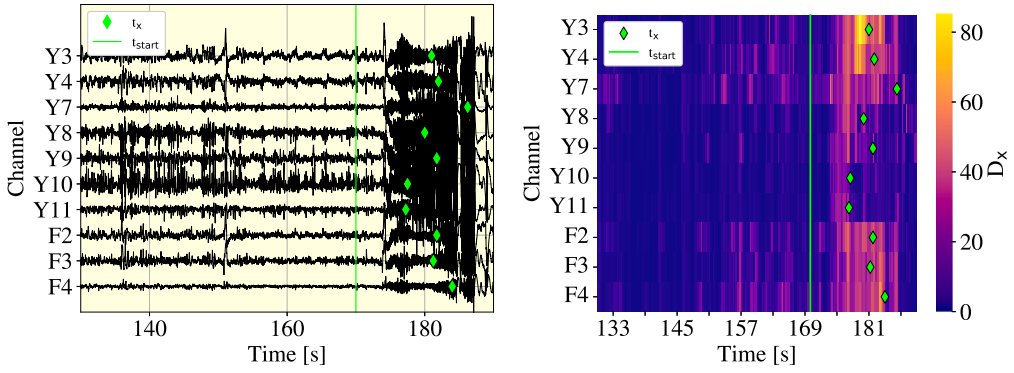

(a) Signal. (b) Desynchronization.

Fig. 4. The DI algorithm (patient 1, $\eta = 40\%$).

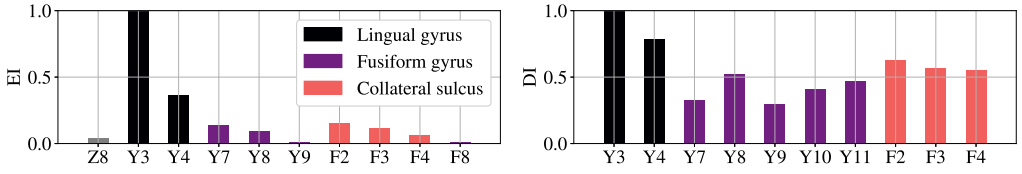

(a) EI. (b) DI.

Fig. 5. EI and DI values for patient 1.

significantly higher than both EI (PR-AUC = 0.43) and DI (PR-AUC = 0.49).[4]

Finally, we conducted a sensitivity analysis on the thresholding method used to distinguish spurious from authentic connectivity phenomena in Section 4.1. Specifically, we computed DI performance in terms of ROC-AUC and PR-AUC by varying the (n_{low}, n_{high}) thresholds across the set $\{(1, 99), (2.5, 97.5), (5, 95), (10, 90), (15, 85), (20, 80), (25, 75)\}$. As shown in Fig. 11, detection performance remains consistent across different thresholds, ranging from a minimum ROC-AUC = 0.84 for $(n_{low}, n_{high}) = (20, 80)$ to a maximum ROC-AUC = 0.87 for $(n_{low}, n_{high}) = (2.5, 97.5)$. The corresponding PR-AUC values are PR-AUC = 0.47 and PR-AUC = 0.52, respectively.

We observe that the best results are obtained by discarding connectivity values that are not statistically significant, using a two-sided test against a null distribution computed from the overall connectivity distribution in the SEEG time-varying network. This demonstrates that our approach implicitly reduces the effect of volume conduction, effectively removing spurious connectivity from the analysis. A summary of the specific performance of each algorithm, including EI and the combined configuration, is reported in Table 2. Notably, the table reports the sensitivity and specificity values corresponding to the best F1 score, obtained while exploring all detection thresholds $\eta \in [0, 1]$.

6. Clinical discussion

The purpose of this study is to validate the hypothesis that the generation of epileptic discharges is associated with a *desynchronization* between the EZ and the rest of the brain. This hypothesis is supported

[4] We observe that, in the figure, the mean ROC and PR curves of the combined algorithm lie below those of the DI algorithm. However, the expectations of the ROC-AUC and PR-AUC of the algorithm combination are higher than that of standalone DI. This discrepancy arises because the mean curves were obtained by interpolating the values of the individual curves for each patient, which can distort the visual representation, whereas the mean ROC-AUC and PR-AUC values provide a more accurate measure of overall performance.

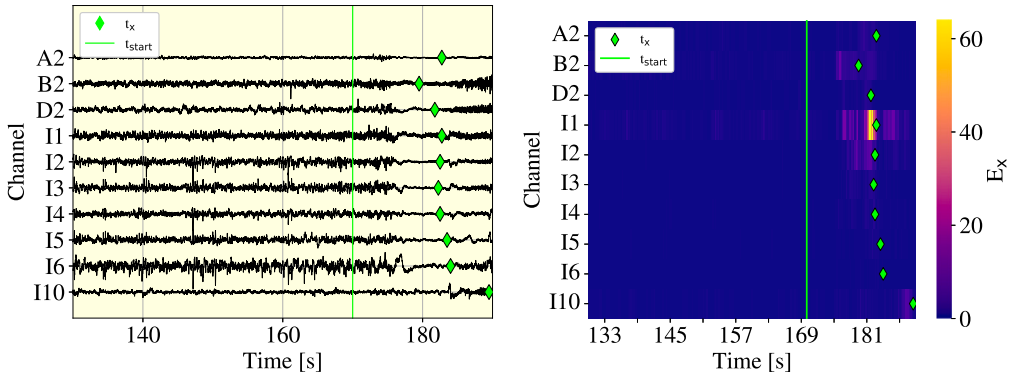

(a) Signal. (b) Energy ratio.

Fig. 6. The EI algorithm (patient 2, $\eta = 6.5\%$).

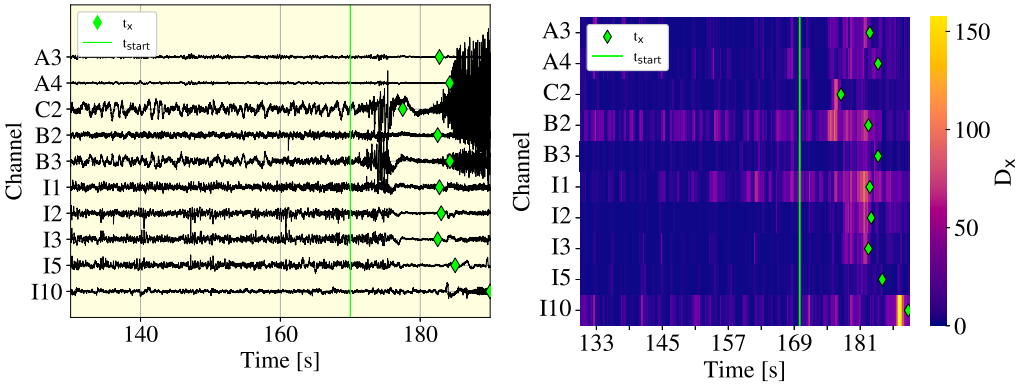

(a) Signal. (b) Desynchronization.

Fig. 7. The DI algorithm (patient 2, $\eta = 11\%$).

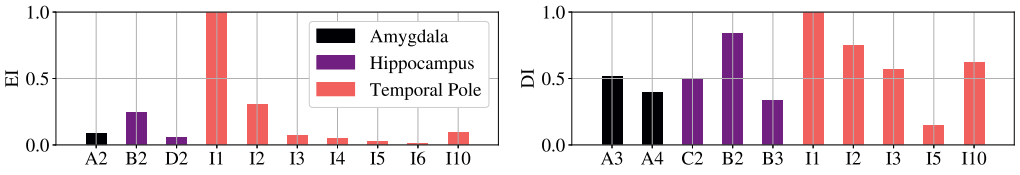

(a) EI. (b) DI.

Fig. 8. EI and DI values for patient 2.

by prior studies [15], but to our knowledge, has not yet been explicitly applied to identify epileptogenic channels in SEEG signals, as implemented by the DI algorithm. The results of the work support our initial hypothesis: DI outperforms state-of-the-art approaches in the localization of the EZ, reinforcing the use of channel desynchronization as a promising biomarker for the analysis of SEEG data.

As PTE estimates the synchrony between neural signals based on the distribution of the instantaneous phase, the DI algorithm identifies as epileptogenic the channels that exhibit a static phase distribution over time and thus are not influenced by other channels in the SEEG implant. From an analytical perspective, our framework assumes that epileptogenic sites exhibit independent behavior that cannot be suppressed by other cortical structures. In this vision, during the interictal phase, the regions surrounding the EZ exert an inhibitory effect, preventing the generation of seizures. Hence, seizure onset occurs when the exchange of information between the epileptogenic and physiological regions is disrupted, consistent with the findings of recent studies [31,41].

In a clinical context, DI is not intended to directly plan the resection area for epilepsy surgery, but rather to support neurophysiologists in the EZ definition. In particular, the combined use of DI and EI can be used to build a first sketch of EZ, allowing neurophysiologists to look at a limited number of channels rather than the entire SEEG network. This could be beneficial in the case of extensive SEEG implants, where understanding the dynamics of seizures is extremely difficult and can lead to fatal human errors. At the same time, the clinical judgment of neurophysiologists remains an essential element in discerning false and true positive, counterbalancing the lower precision of the proposed framework.

We observe that the DI algorithm may implicitly reflect the presence of ictal activity in cortical regions that are not directly sampled by the SEEG electrodes. Since we consider desynchronization as the main biomarker of epileptogenicity, the mere presence of epileptiform waveforms, such as fast oscillations or spikes, diffusely across most SEEG channels is not enough to consider a channel as pathological. In other words, epileptiform activities that do not coincide with a concurrent desynchronization may reflect physiological brain processes or seizure propagation phenomena rather than the true EZ.

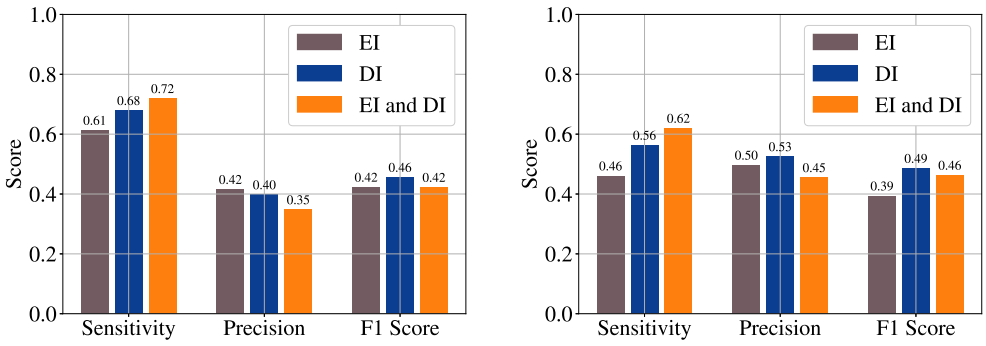

(a) $\eta = 5\%$. (b) $\eta = 10\%$.

Fig. 9. Performance for different detection thresholds.

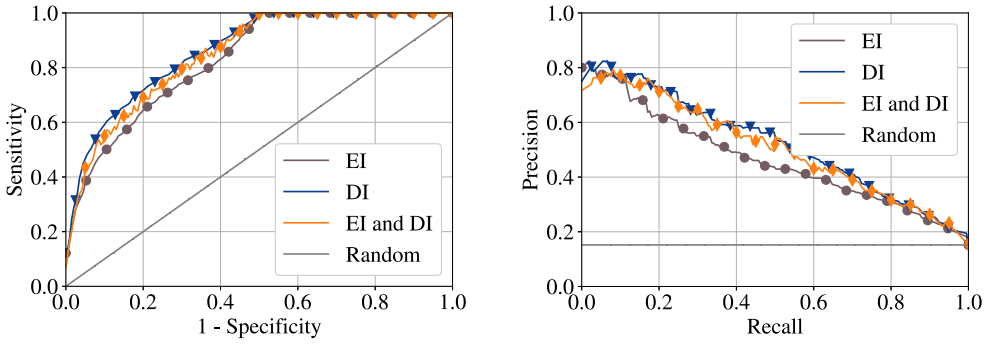

(a) Receiver operating characteristic (ROC) curve. (b) Precision-recall (PR) curve.

Fig. 10. Trade-off between false positives and false negatives.

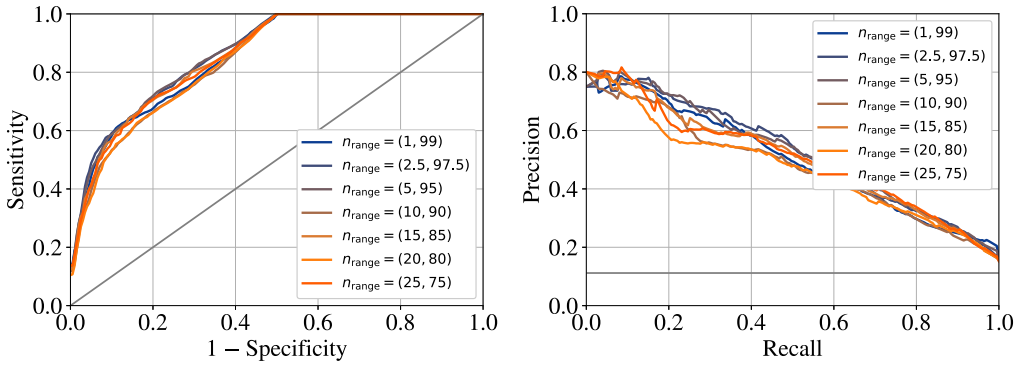

(a) Receiver operating characteristic (ROC) curve. (b) Precision-recall (PR) curve.

Fig. 11. Sensitivity analysis for the Desynchronization Index (DI) algorithm.

From a practical perspective, the presence of channels with high EI values but no corresponding DI values may indicate that the seizure originates from a hidden structure. Therefore, integrating the DI and EI algorithms could distinguish true ictal patterns from the propagation of epileptic discharges, helping neurophysiologists determine whether the epileptogenic network is fully or only partially explored. As a long term objective, the proposed framework could thus be expanded to assess whether the recorded SEEG data provide sufficient information to ensure a high likelihood of successful epilepsy surgery.

We note that our pipeline does not include any pre-filtering stage for the SEEG data, making connectivity information be extracted directly from broadband signals. Consequently, unlike most state-of-the-art approaches, the DI algorithm estimates the connectivity of each SEEG channel considering all its oscillatory components. This enables the algorithm to be implemented in a patient-agnostic manner, without requiring assumptions about the specific waveforms characterizing ictal phenomena, which, notably, may vary from case to case, depending on the location of the EZ [42]. On the other hand, DI can also be tuned to specific frequency ranges, which may further enhance detection accuracy.

Notably, this manuscript considers RFTC channels as the ground truth for the detection framework. In the studied population, thermocoagulated channels accurately targeted epileptogenic tissue, since all RFTC procedures were performed with curative intent and the analysis was restricted to patients who achieved favorable seizures (Engel I–II). Nevertheless, several important limitations should be acknowledged:

Table 2
Performance metrics for different algorithms.

Algorithm	n_{low},n_{high}	ROC-AUC	PR-AUC	F1-Score	Sensitivity	Specificity
	(1, 99)	0.85	0.50	0.55	0.58	0.58
	(2.5, 97.5)	0.87	0.52	0.57	0.59	**0.61**
	(5, 95)	0.86	0.49	0.57	0.61	0.58
DI	(10, 90)	0.84	0.48	0.53	0.61	0.52
	(15, 85)	0.86	0.51	0.55	0.58	0.57
	(20, 80)	0.84	0.47	0.51	**0.65**	0.49
	(25, 75)	0.86	0.50	0.54	**0.65**	0.53
EI	\	0.83	0.43	0.50	0.59	0.51
EI and DI	\	**0.88**	**0.53**	**0.58**	0.62	0.50

RFTC does not provide histopathological validation; spatial sampling is limited by electrode placement; and the selection of RFTC targets is influenced by the need to preserve eloquent cortex, rather than being based solely on epileptogenicity.

In this regard, we note that other studies in this field have often considered the surgically resected area as the clinical ground truth. However, such an approach may not provide an accurate delineation of the EZ, as surgical resections typically cover a region broader than the EZ alone. In our case, selecting thermocoagulated contacts as the detection target is more consistent with the clinical objective of the SEEG evaluation, which is to minimize the extent of cortical tissue resected during surgery and reduce the risk of damaging eloquent structures.

Finally, we observe that the main limitation of this study is the use of a relatively small dataset from a single clinical center. Although our primary objective was to propose a methodology for identifying desynchronization phenomena, extending the analysis to larger datasets will be essential to validate the performance of the DI algorithm and assess its feasibility in real-world scenarios.

7. Conclusions

This work presented a framework for analyzing SEEG signals and, ultimately, improving the likelihood of seizure freedom after epilepsy surgery. We designed a new algorithm, termed Desynchronization Index (DI), which quantifies the epileptogenic level of SEEG channels by measuring the reduction in outward connectivity during the ictal transition. Accordingly, the algorithm considers the ability of a cortical site to behave independently, and thus to *desynchronize* from the brain network, as a key biomarker of the Epileptogenic Zone (EZ).

We evaluated DI on a dataset of 20 patients and compared its performance against the Epileptogenicity Index (EI), which represents the state of the art for identifying the EZ. The results showed that DI leads to a higher Area Under the ROC Curve (ROC-AUC) than EI (AUC = 0.86 vs AUC = 0.83), and combining the two tools improves the AUC by 5.2% with respect to EI (CI: 2.3%–8.0%).

Our results confirm that the desynchronization of SEEG channels represents a key biomarker to identify structures within the EZ. In particular, DI underscores signal modifications that are not visually evident and, when combined with other quantitative biomarkers, may substantially improve the success rate of epilepsy surgery in complex scenarios. In future work, we intend to clinically validate the DI algorithm on a larger dataset, possibly including data from different clinical research centers, and to evaluate the potential of the proposed computational framework for analyzing the inter-ictal period.

CRediT authorship contribution statement

Federico Mason: Writing – review & editing, Writing – original draft, Visualization, Validation, Methodology, Investigation, Formal analysis, Data curation, Conceptualization. **Lorenzo Ferri:** Writing – review & editing, Writing – original draft, Validation, Methodology, Investigation, Formal analysis, Data curation, Conceptualization. **Lidia Di Vito:** Writing – review & editing, Investigation. **Lara Alvisi:** Writing – review & editing, Investigation. **Luca Zanuttini:** Writing – review & editing, Investigation. **Matteo Martinoni:** Writing – review & editing, Investigation. **Roberto Mai:** Writing – review & editing, Investigation. **Francesco Cardinale:** Writing – review & editing, Investigation. **Paolo Tinuper:** Writing – review & editing, Investigation. **Roberto Michelucci:** Writing – review & editing, Investigation. **Elena Pasini:** Writing – review & editing, Supervision, Investigation. **Francesca Bisulli:** Writing – review & editing, Supervision, Investigation.

Declaration of competing interest

The authors declare that they have no known competing financial interests or personal relationships that could have appeared to influence the work reported in this paper.

Data availability

The authors do not have permission to share data.

References

[1] Hans O. Lüders, Imad Najm, Dileep Nair, Peter Widdess-Walsh, William Bingman, The epileptogenic zone: general principles, Epileptic Disord. 8 (2) (2006) 1–9.
[2] Jean Isnard, et al., French guidelines on stereoelectroencephalography (SEEG), Neurophysiol. Clin. 48 (1) (2018) 5–13.
[3] Massimo Cossu, Francesco Cardinale, Laura Castana, Alberto Citterio, Stefano Francione, Laura Tassi, Alim L. Benabid, Giorgio Lo Russo, Stereoelectroencephalography in the presurgical evaluation of focal epilepsy: a retrospective analysis of 215 procedures, Neurosurgery 57 (4) (2005) 706–718.
[4] Francesco Cardinale, Massimo Cossu, Laura Castana, Giuseppe Casaceli, Marco Paolo Schiariti, Anna Miserocchi, Dalila Fuschillo, Alessio Moscato, Chiara Caborni, Gabriele Arnulfo, et al., Stereoelectroencephalography: surgical methodology, safety, and stereotactic application accuracy in 500 procedures, Neurosurgery 72 (3) (2013) 353–366.
[5] Fabrice Bartolomei, et al., Defining epileptogenic networks: contribution of SEEG and signal analysis, Epilepsia 58 (7) (2017) 1131–1147.
[6] Vadym Gnatkovsky, et al., Biomarkers of epileptogenic zone defined by quantified stereo-EEG analysis, Epilepsia 55 (2) (2014) 296–305.
[7] Nicolas Roehri, Jean-Marc Lina, John C. Mosher, Fabrice Bartolomei, Christian-George Bénar, Time-frequency strategies for increasing high-frequency oscillation detectability in intracerebral EEG, , IEEE Trans. Biomed. Eng. 63 (12) (2016) 2595–2606.
[8] Fabrice Bartolomei, Patrick Chauvel, Fabrice Wendling, Epileptogenicity of brain structures in human temporal lobe epilepsy: a quantified study from intracerebral EEG, Brain 131 (7) (2008) 1818–1830.
[9] Olivier David, et al., Imaging the seizure onset zone with stereo-electroencephalography, Brain 134 (10) (2011) 2898–2911.
[10] Abhijit Bhattacharyya, Radu Ranta, Steven Le Cam, Valerie Louis-Dorr, Louise Tyvaert, Sophie Colnat-Coulbois, Louis Maillard, Ram Bilas Pachori, A multi-channel approach for cortical stimulation artefact suppression in depth EEG signals using time-frequency and spatial filtering, IEEE Trans. Biomed. Eng. 66 (7) (2019) 1915–1926.
[11] Meng yang Wang, et al., Identification of the epileptogenic zone of temporal lobe epilepsy from stereo-electroencephalography signals: A phase transfer entropy and graph theory approach, 16, 2017, pp. 184–195,
[12] Timothée Proix, Fabrice Bartolomei, Maxime Guye, Viktor K. Jirsa, Individual brain structure and modeling predict seizure propagation, Brain 140 (3) (2017) 641–654.

[13] Kristin M. Gunnarsdottir, et al., Source–sink connectivity: A novel interictal EEG marker for seizure localization, Brain 145 (11) (2022) 3901–3915.
[14] G. Nithin, P.S. Sathidevi, P.M. Ameer, Graph energy based centrality measures to detect epileptogenic focal invasive EEG electrodes, 85, 2021, pp. 127–137,
[15] Fabrice Bartolomei, Fabrice Wendling, Jean-Jacques Bellanger, Jean Régis, Patrick Chauvel, Neural networks involving the medial temporal structures in temporal lobe epilepsy, Clin. Neurophysiol. 112 (9) (2001) 1746–1760.
[16] Fabrice Bartolomei, Anca Nica, Maria Paola Valenti-Hirsch, Claude Adam, Marie Denuelle, Interpretation of SEEG recordings, Neurophysiol. Clin. 48 (1) (2017) 53–57.
[17] Julia Makhalova, et al., The role of quantitative markers in surgical prognostication after stereoelectroencephalography, Ann. Clin. Transl. Neurol. 10 (11) (2023) 2114–2126.
[18] Alexandra Balatskaya, et al., The ‘‘connectivity epileptogenicity index’’(cEI), a method for mapping the different seizure onset patterns in stereo-electroencephalography recorded seizures, Clin. Neurophysiol. 131 (8) (2020) 1947–1955.
[19] Harilal Parasuram, Siby Gopinath, Ashok Pillai, Shyam Diwakar, Anand Kumar, Quantification of epileptogenic network from stereo EEG, recordings using epileptogenicity ranking method, Front. Neurol. 12 (2021) 738111.
[20] Jean-Philippe Lachaux, Eugenio Rodriguez, Jacques Martinerie, Francisco J. Varela, Measuring phase synchrony in brain signals, Hum. Brain Mapp. 8 (4) (1999) 194–208.
[21] Cornelis J. Stam, Guido Nolte, Andreas Daffertshofer, Phase lag index: assessment of functional connectivity from multi channel EEG and MEG with diminished bias from common sources, Hum. Brain Mapp. 28 (11) (2007) 1178–1193.
[22] Kanupriya Gupta, Pulkit Grover, Taylor J. Abel, Current conceptual understanding of the epileptogenic network from stereoelectroencephalography-based connectivity inferences, Front. Neurol. 11 (569699) (2020) 1–7.
[23] Luis R. Peraza, Aziz U.R. Asghar, Gary Green, David M. Halliday, Volume conduction effects in brain network inference from electroencephalographic recordings using phase lag index, J. Neurosci. Methods 207 (2) (2012) 189–199.
[24] Muriel Lobier, Felix Siebenhühner, Satu Palva, J. Matias Palva, Phase transfer entropy: a novel phase-based measure for directed connectivity in networks coupled by oscillatory interactions, Neuroimage 85 (2) (2014) 853–872.
[25] Fabrice Wendling, Jean-Jacques Bellanger, Fabrice Bartolomei, Patrick Chauvel, Relevance of nonlinear lumped-parameter models in the analysis of depth-EEG epileptic signals, Biol. Cybernet. 83 (4) (2000) 367–378.
[26] Yali Huang, et al., Intracranial electrophysiological and structural basis of BOLD functional connectivity in human brain white matter, Nat. Commun. 14 (3414) (2023) 1–9.
[27] Maëva Daoud, et al., Stereo-EEG based personalized multichannel transcranial direct current stimulation in drug-resistant epilepsy, 137, 2022, pp. 142–151,
[28] John M. Bernabei, et al., Electrocorticography and stereo EEG provide distinct measures of brain connectivity: implications for network models, Brain Commun. 3 (3) (2021) 1–11.
[29] Chunsheng Li, Abbas Sohrabpour, Haiteng Jiang, Bin He, High-frequency hubs of the ictal cross-frequency coupling network predict surgical outcome in epilepsy patients, IEEE Trans. Neural Syst. Rehabil. Eng. 29 (2021) 1290–1299.
[30] André M. Bastos, Jan-Mathijs Schoffelen, A tutorial review of functional connectivity analysis methods and their interpretational pitfalls, Front. Syst. Neurosci. 9 (175) (2016) 1–23.
[31] Haiteng Jiang, et al., Interictal SEEG resting-state connectivity localizes the seizure onset zone and predicts seizure outcome, Adv. Sci. 9 (2200887) (2022) 1–11.
[32] Xiaotong Liu, Fang Han, Rui Fu, Qingyun Wang, Guoming Luan, Epileptogenic zone location of temporal lobe epilepsy by cross-frequency coupling analysis, Front. Neurol. 12 (764821) (2021) 1–14.
[33] Nan An, Xiaolai Ye, Qiangqiang Liu, Jiwen Xu, Puming Zhang, Localization of the epileptogenic zone based on ictal stereo-electroencephalogram: Brain network and single-channel signal feature analysis, 167, 2020, pp. 1–10,
[34] Luiz A. Baccalá, Koichi Sameshima, Partial directed coherence: a new concept in neural structure determination, Biol. Cybernet. 84 (6) (2001) 463–474.
[35] David Freedman, Persi Diaconis, On the histogram as a density estimator: L 2 theory, Z. Wahrscheinlichkeitstheor. Verwandte Geb. 57 (4) (1981) 453–476.
[36] Ross Sparks, James D. Wilson, Monitoring communication outbreaks among an unknown team of actors in dynamic networks, J. Qual. Technol. 51 (4) (2019) 353–374.
[37] Francesco Cardinale, et al., Cerebral angiography for multimodal surgical planning in epilepsy surgery: description of a new three-dimensional technique and literature review, World Neurosurg. 84 (2) (2015) 358–367.
[38] Jr. David W. Hosmer, Stanley Lemeshow, Rodney X. Sturdivant, Applied Logistic Regression, John Wiley & Sons, 2013.
[39] Elena Urrestarazu, Rahul Chander, Francçois Dubeau, Jean Gotman, Interictal high-frequency oscillations (100–500 Hz) in the intracerebral EEG of epileptic patients, Brain 130 (9) (2007) 2354–2366.
[40] Douglas C. Montgomery, Introduction to Statistical Quality Control, John Wiley & Sons, 2019.
[41] Graham W. Johnson, et al., The interictal suppression hypothesis in focal epilepsy: network-level supporting evidence, Brain 146 (7) (2023) 2828–2845.
[42] Stefania Coelli, Eleonora Maggioni, Annalisa Rubino, Chiara Campana, Lino Nobili, Anna M. Bianchi, Multiscale functional clustering reveals frequency dependent brain organization in type II focal cortical dysplasia with sleep hypermotor epilepsy, IEEE Trans. Biomed. Eng. 66 (10) (2019) 2831–2839.